SANDIA REPORT

S A N D 2 0 0 8 - 6 2 8 4
Unlimited Release
Printed September 2008

Dynamic compression of synthetic diamond windows (final report for LDRD project 93531)

Daniel H. Dolan

Prepared by
Sandia National Laboratories
Albuquerque, New Mexico 87185 and Livermore, California 94550

Sandia is a multiprogram laboratory operated by Sandia Corporation,
a Lockheed Martin Company, for the United States Department of Energy's
National Nuclear Security Administration under Contract DE-AC04-94-AL85000.

Issued by Sandia National Laboratories, operated for the United States Department of Energy by Sandia Corporation.

Available to DOE and DOE contractors from
U.S. Department of Energy
Office of Scientific and Technical Information
P.O. Box 62
Oak Ridge, TN 37831

Telephone: (865) 576-8401
Facsimile: (865) 576-5728
E-Mail: reports@adonis.osti.gov
Online ordering: http://www.osti.gov/bridge

Available to the public from
U.S. Department of Commerce
National Technical Information Service
5285 Port Royal Rd
Springfield, VA 22161

Telephone: (800) 553-6847
Facsimile: (703) 605-6900
E-Mail: orders@ntis.fedworld.gov
Online ordering: http://www.ntis.gov/help/ordermethods.asp?loc=7-4-0#online

S A N D 2 0 0 8 - 6 2 8 4 XX
Unlimited Release
Printed September 2008

Dynamic compression of synthetic diamond windows (final report for LDRD project 93531)

Daniel H. Dolan
Dynamic Material Properties
Sandia National Laboratories
P.O. Box 5800
Albuquerque, NM 87185-1195
dhdolan@sandia.gov

Abstract

Diamond is an attractive dynamic compression window for many reasons: high elastic limit, large mechanical impedance, and broad transparency range. Natural diamonds, however, are too expensive to be used in destructive experiments. Chemical vapor deposition techniques are now able to produce large single-crystal windows, opening up many potential dynamic compression applications. This project studied the behavior of synthetic diamond under shock wave compression. The results suggest that synthetic diamond could be a useful window in this field, though complete characterization proved elusive.

Acknowledgments

This project would not have been possible without synthetic diamond samples provided by the Carnegie DOE Alliance Center and Apollo Diamond. In particular, I would like to thank Russ Hemley, Bill Dromeshauser, Al Genis, and Pat Doering for their efforts in this area.

Suzi Grine-Jones performed most of the sample characterization and assembly, with assistance from Andrew Shay. Ultrasonic wave speed measurements were made by Steven Younghouse. Laue diffraction measurements were performed by Dan Hooks.

All experiments were performed at the Sandia STAR facility. Bill Reinhert, Tom Thornhill, and John Martinez were responsible for carrying out these experiments. Their help in designing and completing a variety of non-standard experiments is appreciated.

Jason Podsednik built and fielded the fast VISAR and three-phase PDV measurements in this project. An additional fixed cavity VISAR was obtained from Brian Jensen. Conventional PDV measurements were supported by Scott Walker and Ed Marsh.

Steve Sheffield, David Holtkamp, Marcus Knudson, Scott Jones, Jim Asay, and Tracy Vogler provided helpful technical discussions throughout this project.

This work was performed under the Sandia LDRD program (project #93531). Sandia is a multiprogram laboratory operated by Sandia Corporation, a Lockheed Martin Company, for the United States Department of Energy's National Nuclear Security Administration under Contract DE-AC04-94AL85000.

Table of Contents

List of Figures

List of Tables

CHAPTER 1
Introduction

Optical windows are an important component of dynamic compression research. Without an appropriate window, measurements of opaque materials (*e.g.*, metals) are restricted to the free surface, where the stress is always zero. To maintain non-zero stress, the sample under study must be covered with a well characterized, well behaved window material. In many cases, the window's operating range constrains the measurements that can be performed in a dynamic compression experiment.

This report describes research into synthetic diamond as a dynamic compression window, a project spanning three years (FY 2006–2008) under the Sandia LDRD program. The following sections describe the motivation and research activities for this project. The organization of subsequent chapters in this report is also provided.

1.1 The need for diamond windows

A useful dynamic compression window is defined by three general requirements:

1. The material must be transparent.
2. The material must be easily understood and modeled.
3. The material must be sufficiently robust.

The precise meaning of each requirement is application specific, but there are several general qualifications. Visible/near-infrared transparency is needed because optical velocimetry is typically performed in this spectral range. Windows must also be free from phase transitions and either be completely elastic (or overdriven into their plastic state) over some useful range. Finally, window materials should tolerate their intended application. For example, sapphire is a reasonable window for aqueous samples, but NaCl is not.

The above requirements are by no means the only considerations in the selection of a dynamic compression window. Mechanical impedance (the product of density and wave speed) is often a very important factor in experiment design; thermal conductivity is another.

Since dynamic compression is typically destructive, material availability and cost are also relevant.

Nearly all dynamic compression research is performed with the following windows: silica (crystalline or amorphous), alumina (sapphire), and lithium fluoride. The two oxides are typically used in their elastic domain (< 8 GPa and < 18 GPa, respectively), while lithium fluoride is used in its plastic domain (1–150 GPa). Although lithium fluoride covers a wide stress range, there are many circumstances where it is not a suitable window. At low stresses (< 10 GPa), impure/misaligned lithium fluoride is not completely overdriven and has a time dependent response [1, 2]. Lithium fluoride has a relatively low mechanical impedance (comparable to aluminum), is not very stable to thermal stress, and is somewhat water soluble. In most regards, sapphire is a much better dynamic compression window than lithium fluoride, but is limited by inelastic deformation.

Diamond is an ideal window in many situations, but the high cost of natural diamond prevents its use in dynamic compression research. However, diamond synthesis technologies have reached a point where modest diamond crystals (≈ 1 mm thick) are generally feasible. This project was initiated to study the usefulness of synthetic diamond as a dynamic compression window.

1.2 Project overview

The fundamental goal of this project is to determine the usefulness of synthetic diamond as a dynamic compression window. The information needed to make this determination includes the elastic limit, the mechanical response (Hugoniot), and the window correction (for optical velocimetry). This information can be obtained from symmetric impact experiments, where one diamond window strikes another window at a known velocity.

A crucial step in this study was obtaining sufficiently large diamonds for useful impact experiments. Such diamonds were relatively scarce at the beginning of this project, and the supply remains limited (though production capacity is increasing). In preparation for the symmetric diamond experiments, cubic zirconia [3] was used as a surrogate material. When sufficient amounts of diamond windows were on hand, characterization and impact experiments began, following protocols developed for cubic zirconia.

Another important aspect of this project is the development of high speed velocimetry. Previous studies of diamond [4] found that precise characterization of the elastic limit was hampered by the diagnostic time resolution. Several approaches in this project were tried to circumvent these limitations.

1.3 Chapter organization

The following chapters provide a comprehensive description of this project. Background information about diamond and shock wave research is given in Chapter 2. Experiments

completed during this project are described and analyzed in Chapter 3; less developed, ongoing efforts are discussed in Chapter 4. A project summary and recommendations for future work are given in Chapter 5

CHAPTER 2
Background

This chapter provides background information relevant for this project. First, a summary of previous shock wave studies of diamond is presented. Next, a brief survey of diamond synthesis is given. Finally, the symmetric impact experiment, used extensively throughout this project, is described.

2.1 Properties of diamond

Aside from the being the hardest known substance, diamond is an interesting and unique material. Diamond has a fairly low density (3.51–3.52 g/cc) but a high acoustic wave speed ($\sim$ 17.5–18 km/s), so it's mechanical impedance (62–63 GPa/(km/s)) is exceeds that of tantalum (57 GPa/(km/s)) and gold (59 GPa/(km/s)). The elastic range of diamond exceeds 50–100 GPa (depending on orientation), much larger than any other known material.

Pure diamond (type IIa) can be used as a window throughout most of the visible, infrared, and x-ray spectrum [5]. In the infrared, diamond has an intrinsic absorption band in range of 2–6 μm, and the presence of nitrogen impurities leads to 6–12 μm absorption as well. The ultraviolet absorption edge of diamond is 222 nm for ultrapure diamond, 291 nm for type Ia diamond (which contains nitrogen impurities).

Other distinguishing properties of diamond include its chemical robustness and its remarkable thermal conductivity. Unlike many infrared window materials, diamond is resistant to most chemical reactions, although it can be made to oxidize at high temperature. Diamond is also hydrophobic, whereas most insoluble window materials (*i.e.* oxides) are hydrophilic. Diamond is also an exceptional thermal conductor ($K > 1000$ W/m·K), exceeding copper and silver by a considerable margin.

2.2 Previous studies of shock compressed diamond

Diamond anvils are a standard component in static high-pressure research [6]. With the proper design, diamond can be used as an anvil for pressures beyond 100 GPa [6, 7]. Figure 2.1 illustrates the conceptual operation of a diamond anvil cell.

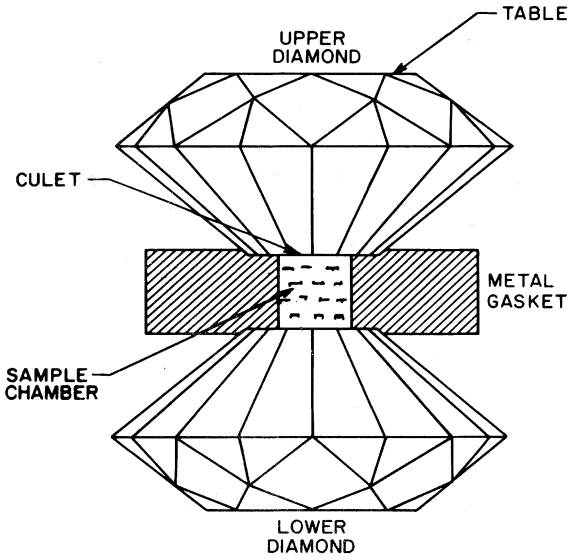

Figure 2.1. Conceptual drawing of the diamond anvil cell (from Reference 6).

In contrast, very little is known about the elastic behavior of diamond under shock compression, largely due to the high cost of natural diamond crystals. The first comprehensive study of diamond crystals under shock compression was made by Boteler and Gupta [8, 9]. This work focused on changes in the Raman spectrum of diamond crystals shocked along different orientations, along with some continuum modeling. The elastic Hugoniot of diamond was predicted using finite strain theory (units of km/s).

$$U_s = 17.55 + 0.5u_p \qquad \langle 100 \rangle \text{ orientation} \tag{2.1}$$

$$U_s = 18.33 + 1.7u_p \qquad \langle 110 \rangle \text{ orientation} \tag{2.2}$$

Based on the reversibility of the Raman spectra during unloading, it appears that diamond remains elastic to at least 40–45 GPa (higher stresses were not studied).

A previous Sandia LDRD [4] sought to investigate the mechanical properties of diamond crystals under shock compression. Two-wave structure was observed when a shock was propagated along $\langle 110 \rangle$ orientation, with an estimated elastic precursor of 90–100 GPa. This value roughly corresponds to molecular dynamics simulations [10], which estimate the elastic limit at 125 ± 15 GPa for the $\langle 100 \rangle$ orientation. Due to diagnostic limitations at that time, VISAR (Velocity Interferometer System for Any Reflector) [11] measurements were limited to 1–2 ns, making precise determination of the elastic limit impossible.

2.3 Synthetic diamond crystals

Since dynamic compression experiments are typically destructive, a low cost alternative to natural diamond is needed. Recent advances in diamond synthesis bring the possibility of inexpensive diamond windows closer to reality. A brief overview of diamond synthesis is presented here, along with the characterization of the diamonds used in this project.

2.3.1 Fabrication

Synthetic diamond has been available since mid-1950's [12] in powder form for industrial applications. Large, single-crystal synthetics are much more difficult to fabricate, and are available in limited quantities. Two methods can be used to create large synthetic diamonds: high pressure/high temperature (HPHT) processes and chemical vapor deposition (CVD).

HPHT diamond growth follows similar principles as industrial diamond synthesis [13]. A carbon source (preferably industrial diamond) placed within a metal solvent inside a high-pressure chamber exposed to a slight thermal gradient. The carbon source, located at the highest temperature, dissolves into the metal solvent. A diamond seed, located at a lower temperatures location, induces crystal growth as carbon precipitates out the solution. Three carat diamond crystals[1] using this approach [14], although the material tends be colored (typically yellow) due to residual nitrogen impurities.

CVD diamond synthesis has traditionally been used to create thin (0.001-0.1 mm) diamond coatings, but can be optimized to yield large, single-crystal windows oriented along the $\langle 100 \rangle$ direction [15]. A low-pressure microwave plasma generated in chamber containing methane (with small amounts of nitrogen or oxygen) deposits crystalline diamond at a rate of 0.010–0.100 mm/hour. The process requires a crystal seed, which is cut away after growth is complete. Unlike HPHT diamonds, CVD diamonds are nearly colorless.[2] Diamonds up to 10 ct in size have been fabricated with CVD techniques [16].

To avoid optical absorption, the project used CVD diamonds rather than HPHT materials. Diamond windows were obtained from two suppliers, Apollo Diamond and Carnegie DOE Alliance Center (CDAC), using similar (though proprietary) growth techniques. Figure 2.2 shows a photographs of windows obtained from both suppliers during the course of this project. The windows were separated from the growth substrate and polished on both sides. Initially, the windows were roughly rectangular in shape, with the outer layer covered in a residual carbon layer. Over time, laser milling was used to shape the windows into a round, uniform diameter.

[1] By definition, a 1 carat (ct) diamond weighs 200 mg. For comparison, a 5 mm diameter, 1.25 mm thick plate (characteristic of this study) is about 0.43 ct. The ideal size for routine impact applications (1" diameter, 1/4" thick) would be a 54 ct diamond!

[2] Trace amounts of nitrogen used to enhance the growth rate of CVD diamonds may leave a slight brown-gray tint. High pressure, high temperature annealing can reduce these effects [15], but were not employed in this work.

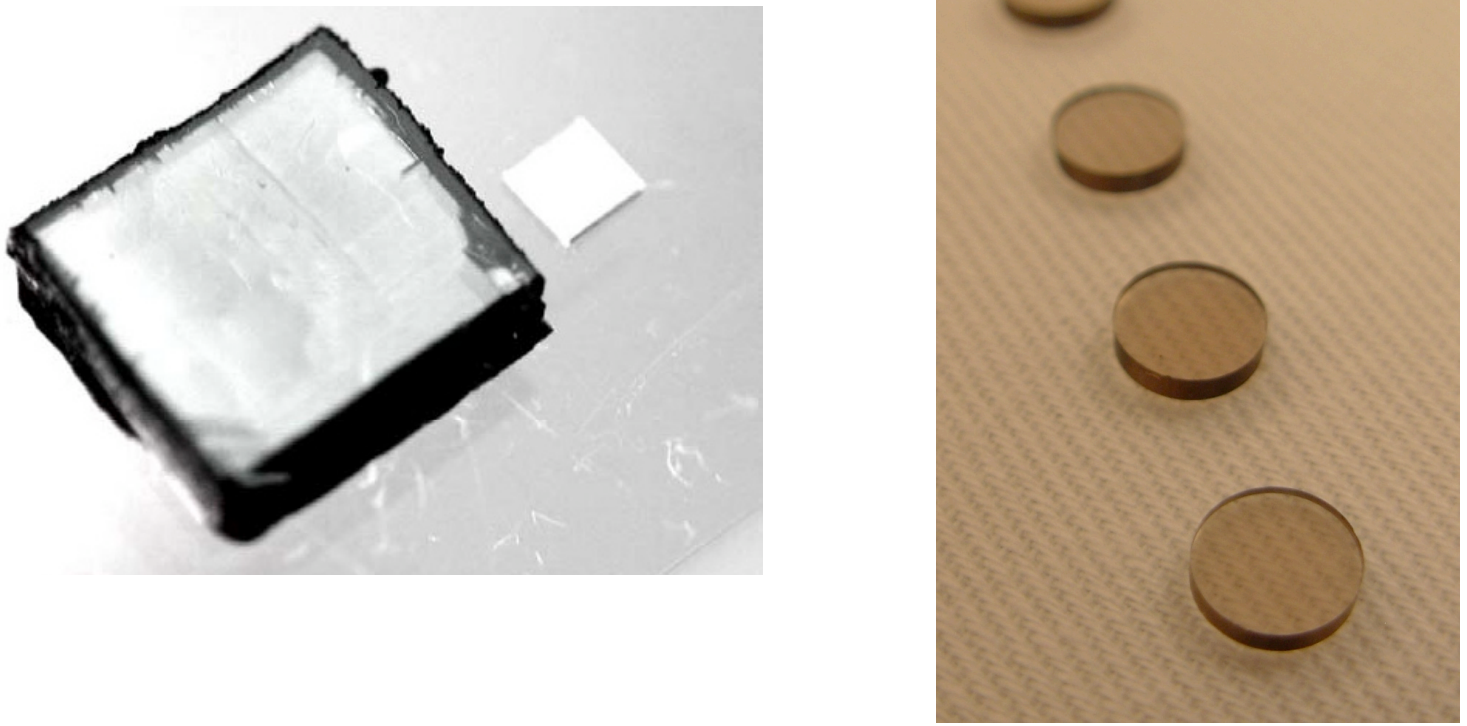

Figure 2.2. (left) A $7 \times 7 \times 2$ mm CVD diamond from CDAC. The dark carbon edges are characteristic of samples obtained at the beginning of this project. A commercial $2 \times 2 \times 1$ diamond plate is shown for comparison. (right) Four CVD diamonds (5 mm diameter, 1 mm thick) from Apollo Diamond.

Table 2.1. Wave speed measurements of ⟨100⟩ synthetic diamond windows

	v_L (km/s)	v_T (km/s)
CDAC	17.56 ± 0.08	12.88 ± 0.04
Apollo	17.72 ± 0.16	12.91 ± 0.09
Boteler	17.53	12.83

2.3.2 Characterization

The limited size and residual carbon edges of the synthetic diamond windows made precise sample characterization extremely difficult. Dimensional characterization was performed with a Nikon NEXIV system (non-contact). These measurements revealed significant wedge (0.2–0.3°) in may of the initial pieces. Sample parallelism improved over time, but remained a point of concern in target fabrication.

Continuum density measurements were not attempted in this project for two reasons. First, the residual carbon boundary on many of the windows would contaminate the measurement, both by having a different density than the bulk material and by trapping air bubbles when submerged in a reference liquid. Second, the relatively small window mass (< 100 mg) did not seem sufficient for precise density measurements.

Laue diffraction measurements were performed on a few diamond samples (AD11–AD19) to confirm the ⟨100⟩ orientation. Figure 2.3 shows a representative diffraction pattern from sample AD19. The samples appear to be nearly oriented along the ⟨100⟩ axis, but no quantitative analysis was performed.

The longitudinal and transverse wave speeds of several synthetic diamond samples were measured by ultrasound techniques. The average results for each material supplier are shown in Table 2.1. Calculated wave speeds from Boteler [17] are also shown for comparison. The the measurements agree within uncertainty, and deviate from previous studies by $\lesssim$1%.

2.4 Symmetric impact of optical windows

Symmetric impact experiments were the primary technique used in this project to study the shock behavior of synthetic diamond. The conceptual layout of a symmetric impact experiment is shown in Figure 2.4. In this experiment, impactor A is driven into an identical target B at a velocity v. Upon impact, symmetric shock waves created in both materials travel at velocity U_s, while the interface between the impactor and target travels at velocity u. Since the target material is transparent, the interface velocity can be measured with optical interferometry, aided by an Al mirror deposited at this location.

Figure 2.3. Laue diffraction pattern (25 keV) of diamond sample AD19

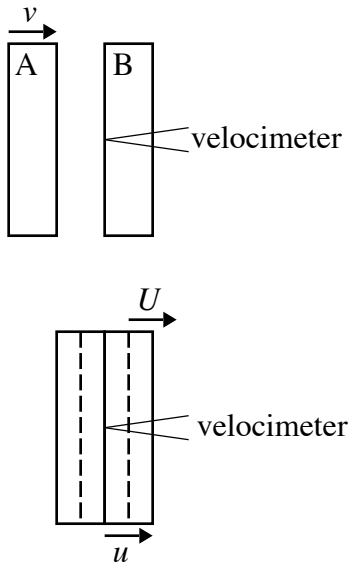

Figure 2.4. Conceptual layout of a symmetric impact experiment. The upper drawing shows the experiment just prior to impact, while the lower shows the experiment just after impact.

The benefits of window characterization by symmetric impact are twofold. First, the experiment symmetry forces $u = v/2$, regardless of the mechanical response of the material. Impact velocity can be measured to high precision ($< 1\%$), so the interface velocity is well known. Second, the shock transit time can be determined from a single optical diagnostic with extremely high accuracy: sub-nanosecond uncertainties are easily achieved. With precise measurements of the target thickness, each symmetric impact experiment can yield a high precision Hugoniot state. Furthermore, the window correction of the target material can be determined at the same time.

The use of symmetric impact to characterize diamond builds upon several previous studies. The method has been used with VISAR to study quartz [18], sapphire [19] and lithium fluoride [20]. As part of this project, similar techniques were used to characterize cubic zirconia [3]. Symmetric impact experiments using Photonic Doppler Velocimetry (PDV) measurements have also been applied to standard window materials (quartz, sapphire, and lithium fluoride) [21]; techniques and analysis from that work are also implemented here.

CHAPTER 3

Shock compression of synthetic diamond

The symmetric impact experiments described in this chapter form the bulk of this project. The following sections describe various aspects of these experiments. First, details of the sample/impactor construction and diagnostic setup are presented. Next, results from specific experiments are discussed. Finally, the experimental results are collated and analyzed to reveal the mechanical and optical behavior of shocked synthetic diamond.

3.1 Experiment overview

Table 3.1 summarizes the symmetric impact experiments performed in this study. All experiments were performed on the STAR two-stage gun. Two synthetic diamond windows were consumed in each experiment: one as the impactor, the other as the target. Construction details for both pieces are given below. VISAR or PDV diagnostics tracked the impact surface between the two diamond windows.

For each experiment, targets and impactors were individually matched using windows from the same material batch. Higher quality diamonds are needed for the impactors because light passes through this material as part of the VISAR/PDV measurement. No definitive protocol was developed, but targets were chosen to have higher clarity, parallelism, and shape uniformity than the impactors. Targets and impactors with similar limiting diameters were used to make optimal use of the limited material stock.

3.1.1 Target construction

All diamond targets in this work were completely coated on one side with Al. This coating acted as the primary reflector in the VISAR/PDV measurements. Complete coating, rather than a small (1-2 mm) spot, was used because of the difficulty in centering coating spots on irregularly shaped windows.[1] In experiments with VISAR diagnostics, an anti-reflective coating (centered at 532 nm) was applied to the opposite side of the the diamond window; anti-reflective coatings were *not* used for PDV measurements.

[1] Window irregularity was particularly problematic in the first two years of this project

Table 3.1. Symmetric impact experiments using synthetic diamond ($\langle 100 \rangle$ orientation). For each diamond window, the thickness and limiting diameter are listed in mm. The first group of experiments used a fast VISAR diagnostics, while the second group used PDV.

Experiment	Impactor	Target	v_{imp} (km/s)
SSD1	AD2	AD1	1.601
	(0.890×4.9)	(1.337×4.7)	
SSD2	AD3	AD4	1.503
	(0.980×4.0)	(1.094×4.5)	
SSD3	CD2	CD1	1.502
	(1.245×5.3)	(1.609×6.9)	
SSD6	AD12	AD17	1.691
	(1.034×4.6)	(1.151×5.05)	
SSD7	AD13	AD18	1.778
	(0.915×4.8)	(1.090×5.00)	
SSD8	AD14	AD19	1.594
	(1.184×4.8)	(1.145×5.03)	
SSD10	AD22	AD23	0.971
	(1.199×4.99)	(1.366×4.98)	

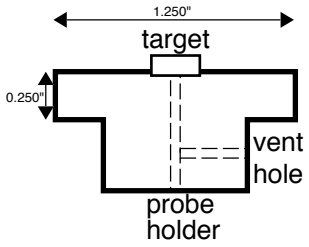

Figure 3.1. Target mount for symmetric impact experiments

Many of the diamond windows, particularly in the beginning of this project, had a noticeable wedge angle (0.1–0.5°). Diamond targets were bonded to an aluminum mount, which could be machined to compensate for wedge and guarantee normal impact. The design of the mount evolved over time, but the basic concept is illustrated in Figure 3.1. The diamond was held in a counter bore on one side of the mount, with optical access and vacuum venting on the other side (the mount shown in Figure 3.1 holds a needle probe). The counter bore was custom machined slightly larger than the diamond target, which was visually centered and bonded into the counter bore. Once the bond was set, the mount was placed in a lathe with the diamond facing away from the chuck. By bouncing light from a laser pointer off of the exposed diamond surface, the mount was aligned with the rotation axis of the lathe. An minor cut (0.001–0.002") was made on the front of the mount to provide an alignment surface for final assembly. The alignment surface of mount was verified to be parallel to the diamond impact surface within 1–2 mrad.

To maintain impact centering, the target mount was slid into a centered hole of a target plate on the two-stage gun. The target plate was centered with a precision madrel installed in the barrel of the two-stage gun; the hole in target plate had precisely the same diameter as the madrel, which was the same size as the barrel's inner diameter. The target mount, being slighly smaller than the hole, was wrapped in cellophane tape and pressed into the target plate. The mount was pushed until the alignment surface (described above) contacted a set of gauge blocks resting on the barrel of the two-stage gun. Using this approach, the target was thought to be centered to better than 0.100 mm; impact tilt was in the range of 0.5–8 mrad, characteristic of two-stage gun in this operation mode. Though the mount is held quite securely by friction with the target plate, five-minute epoxy was added the rear surface to ensure that the mount remained fixed until impact.

3.1.2 Impactor construction

Diamond impactors were bonded to an aluminum disk to compensate for the wedge angle. The disk itself had a shallow counter bore for centering, and was much smaller than the target mount ($\approx$ 12 mm outer diameter). Alignment cuts were made in a similar fashion

as the target mount, except that the cut was made on the *opposite* side of the mount. The impactor mount was held in the lathe check, diamond facing the spindle, with laser light coming in and out of the spindle. After the alignment cut was complete, the impactor mount was bonded into a centered counter bore on the final projectile of the two-stage gun.

3.1.3 Diagnostics

The terminal velocity of the projectile was determined with the Optical Beam Reflectance (OBR) system of the two-stage gun. This system detects the passage of the projectile through fixed intervals by an optical method accurate to about 0.1% [22].

The apparent velocity of the impact surface was determined with either a VISAR or PDV measurement. VISAR measurements were made with a custom-built push-pull system. This VISAR is conceptually similar to the STL fast VISAR operated at the Z/ZR facility, though this is a single channel system, using un-amplified photodiodes and CW laser light. A focusing probe from Oz Optics, held in an adjustable tilt/pan mount, was used in all VISAR measurements. PDV measurements were made with an all fiber system from National Security Technologies. Bare fiber probes (also provided by National Security Technologies) were inserted directly into the target mount. The probes were angle polished to limit the probe's back reflection at -50 to -60 dB.

3.2 VISAR measurements

Three symmetric diamond experiments were performed using VISAR diagnostics. The intent of these experiments was to obtain precision Hugoniot points and window correction values for stresses on the upper end of previous shock work [9]. Since diamond has such a large mechanical impedance, obtaining low pressure states turned out to be quite difficult on the two-stage gun, which typically operates at 2–10 km/s.

3.2.1 Experiment SSD1

Experiment SSD1 was performed with two Apollo Diamond windows: AD2 (the impactor) and AD1 (the target). The impact velocity in this experiment was 1601 km/s. The VISAR system was configured with a fringe constant of 1075 km/s.

Figure 3.2 shows the VISAR measurement results from this experiment. At impact, apparent velocity jumps to 1577 ± 11 m/s and there is loss of contrast. The impact state is held for 74.8 ± 0.3 ns, until the shock reaches the target's free surface. The negative velocity observed after free surface breakout is an apparent velocity effect—the impact surface itself does not actually turn around.

The constant velocity and contrast between impact and free surface release suggests that the diamond target remained elastic in this experiment. There may be some structure in the free surface release, but it is not clear if this is signal of wave splitting in the diamond

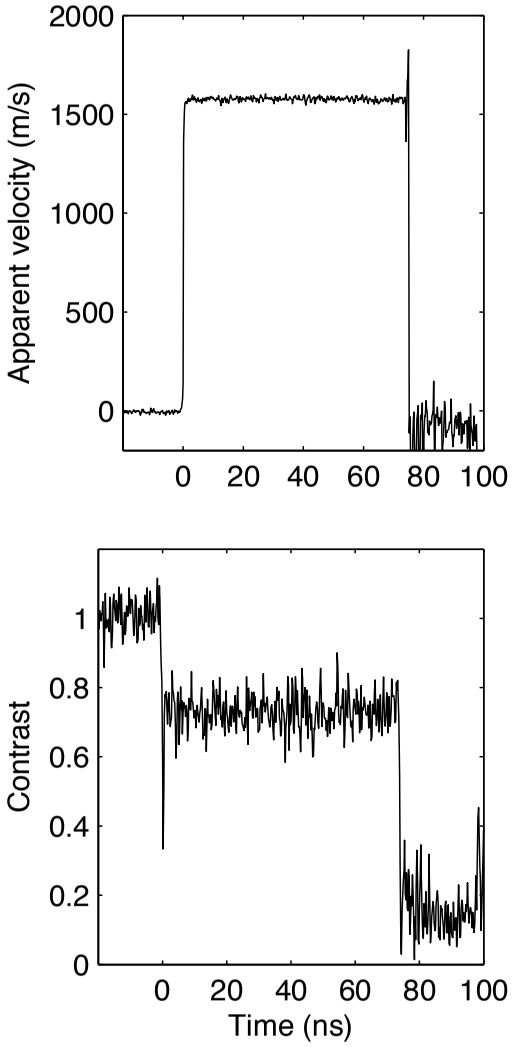

Figure 3.2. VISAR results from experiment SSD1

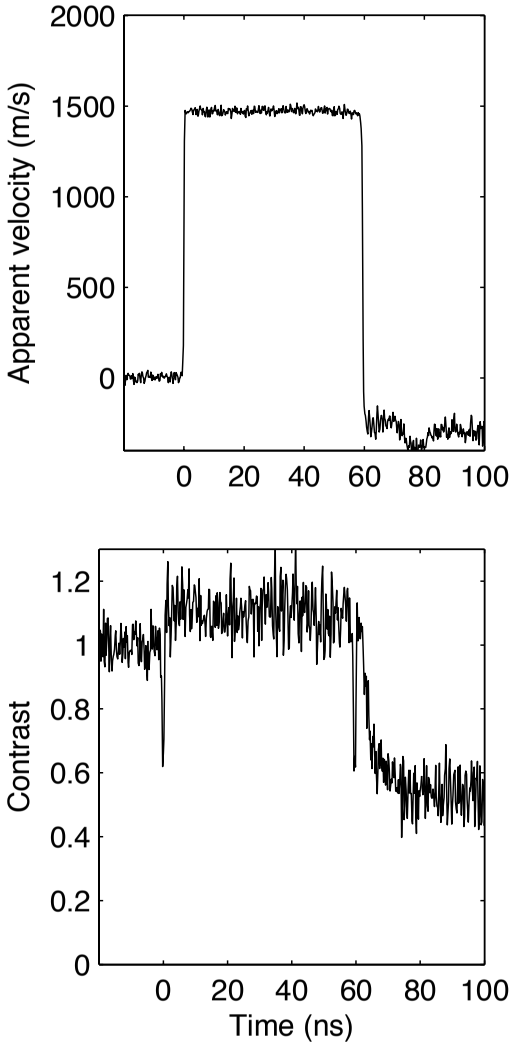

Figure 3.3. VISAR results from experiment SSD2

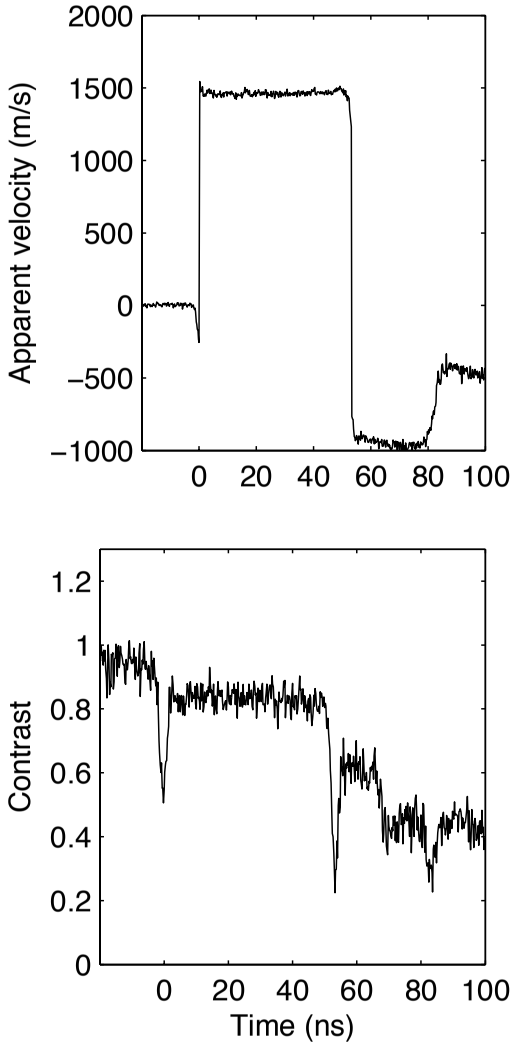

Figure 3.4. VISAR results from experiment SSD3

target or launch/ringing of the anti-reflective coating.

3.2.2 Experiment SSD2

Experiment SSD1 was performed with two Apollo Diamond windows: AD3 (the impactor) and AD4 (the target). The impact velocity in this experiment was 1503 km/s. The VISAR system was configured with a fringe constant of 1825 km/s.

Figure 3.3 shows the VISAR measurement results from this experiment. At impact, apparent velocity jumps to 1474 ± 16 m/s and there is loss of contrast. The impact state is held for 59.5 ± 0.3 ns. As in the previous experiment, contrast remains constant as the shock wave propagates through the diamond target. More release structure is evident in the this experiment than in SSD1.

3.2.3 Experiment SSD3

Experiment SSD3 was performed with two CDAC windows: CD2 (the impactor) and CD1 (the target). The impact velocity in this experiment was 1502 km/s. The VISAR system was configured with a fringe constant of 1825 km/s.

Figure 3.4 shows the VISAR measurement results from this experiment. At impact, apparent velocity jumps to 1462 ± 15 m/s and there is loss of contrast. The impact state is held for 53.2 ± 0.3 ns. Unlike SSD1–SSD2, free surface release in this experiment is soon followed by a strong apparent velocity jump.

3.2.4 Summary of VISAR measurements

Initially, the results from all three VISAR experiments seem to be generally similar: apparent velocity jumps to a steady state, followed by an apparent velocity drop at the beginning of free surface motion. However, if the shock velocity was similar in all three experiments (≈ 18 km/s), then the free surface release should have occurred around $t = 90$ ns, not $t = 53$ ns. Furthermore, the apparent velocity after free surface release is substantially more negative in SSD3 than in SSD2 or SSD3. However, the fact that all experiments show relatively constant contrast during between the two events rules out substantial inelastic effects.

A plausible explanation for the results of SSD3 is that the probe was pointed far from the sample center. An unfortunate limitation of these experiments is the inability to accurately see where the probe points. Instead, one can only move/orient the probe mount to optimize light return. If the probe region were far off center, it is quite possible that velocity feature after impact is not free surface release, but instead corresponds to lateral release (*i.e.*, edge wave). An attempted repeat of experiment SSD3 was cancelled due to a sudden signal loss during setup. Later inspection found a laser burn near the sample edge, supporting the idea that the probe may become grossly misaligned. In most experiment set ups, the

probe is initially centered and aligned with the target's central axis. Perhaps the angular compensation needed to obtain maximum light return in a highly wedge sample steers the probe spot too far off center?

Signal limitations are another problem with the fast VISAR measurement. Even when running with maximum laser power (2–5 W), we were often unable to obtain more than 10–20 mV signals, which is on the low end of fast digitizer sensitivity. Pushing more CW power through fiber runs the risk of burning, which occurred several times during the experiment set up. Because of these limitations, only one VISAR channel could be fielded at a time, making redundant measurements with different fringe constants impossible.

3.3 PDV measurements

Later symmetric impact experiments used PDV rather than PDV for several reasons. First, the signal limitations described in the last section could not be overcome without either sacrificing time resolution (using photo-multiplier tubes) or synchronizing a pulsed laser source with the two-stage gun.[2] Another advantage of PDV measurements is that an anti-reflective coating is not needed on the free surface—PDV can accommodate multiple Doppler shifts where VISAR cannot. The removal of this coating eliminates potential complications, such as ringing and/or coating launch, during free surface release.

3.3.1 Experiment SSD6

Experiment SSD6 was performed with two Apollo Diamond windows: AD12 (the impactor) and AD17 (the target). The impact velocity for this experiment was 1.691 km/s, somewhat higher than previous experiments due to a powder blend change in the first gun stage.

Figure 3.5 shows the results from the PDV measurement in this experiment. The upper plot is the raw signal data, with the time of impact and free surface motion indicated; the transit time between these events is 62.1 ± 0.2 ns. The middle plot shows a time-frequency analysis of the data, which is calculated via a short-time Fourier transform with a 15 ns Gaussian window (padded to 2048 points, 1025 frequency bins); the DC level is subtracted out before performing the transform, so periods of zero motion do not show up in the image. An inverted linear grayscale is used in this image, so dark areas indicate strong spectral features. The lower plot shows the average spectral profile for times between 10 and 50 ns (indicated by dashed lines). The peak location, determined via Gaussian fit, is 1663 ± 2 m/s.

The velocity jump after impact and the two strong features after free surface release can be linked to the impact surface velocity, the free surface velocity, and the window correction [21]. The apparent velocity after impact is simply av, where a is the window correction (1.967 in

[2]While not impossible, synchronization with the two-stage gun is difficult since most triggering is done after impact. The variation of velocity between shots (particularly below 2 km/s) make it very easy for lasers trigger prior to impact to miss the event entirely.

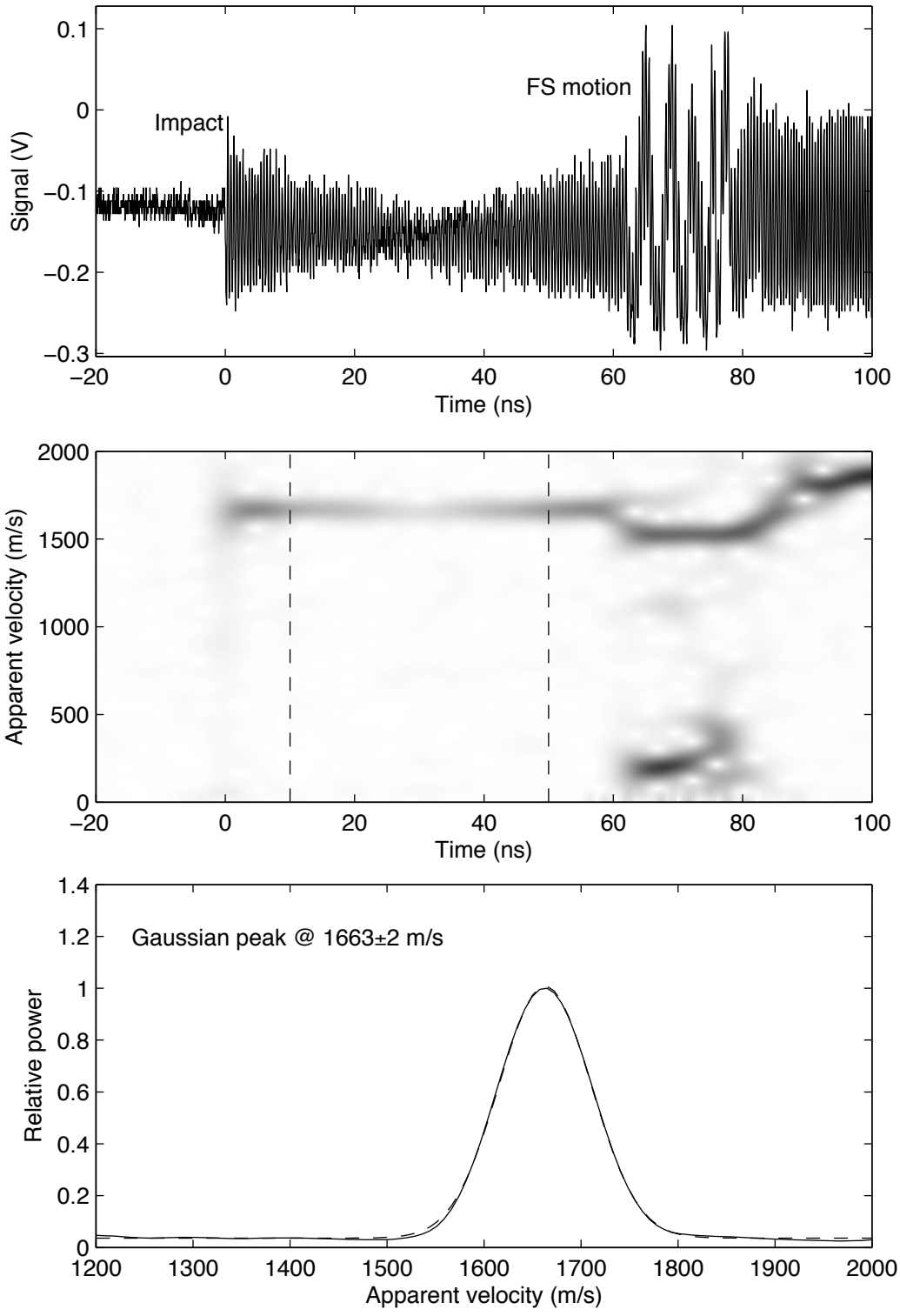

Figure 3.5. PDV results from experiment SSD6

this spectrogram). For an elastic material, the features after free surface release should be at $(2a-2)u$ (1635 m/s) and $|2-a|u$ (28 m/s). However, the free surface release features in Figure 3.5 occur at 1529 and 212 m/s, which implies that the compression is not entirely elastic. Inelastic behavior can also be inferred by the decrease in fringe amplitude after shock impact; subsequent return of fringe amplitude is probably due to increasing probe efficiency as the target moves closer to the bare fiber.

3.3.2 Experiment SSD7

Experiment SSD7 was performed with two Apollo Diamond windows: AD13 (the impactor) and AD17 (the target). The impact velocity was 1.778 km/s.

Figure 3.6 shows the results for this experiment, analyzed in the same fashion as experiment SSD6. After impact, there is a short lived feature near 1779 ± 22 m/s, visible for only 10–15 ns before the sample becomes opaque. The sample remains opaque until free surface release (59.5 ± 0.2 ns after impact), at which point the PDV tracks the free surface motion. The motion of this surface is fairly complicated for about 50 ns, eventually setting to a steady state near 1120 m/s. The total loss of light from the impact surface indicates the diamond underwent substantial inelastic deformation, presumably followed by the formation of optical scattering sites [23].

3.3.3 Experiment SSD8

Experiment SSD8 was performed with two Apollo Diamond windows: AD14 (the impactor) and AD19 (the target). The impact velocity was 1.594 km/s.

Figure 3.7 shows the results for this experiment, analyzed in the same fashion as experiment SSD6. After impact, the PDV signal indicates a steady apparent velocity of 1572.7 ± 0.1 m/s for a duration of 62.8 ± 0.1 ns, at which point free surface motion begins. Applying the same analysis described for experiment SSD6, the window correction is roughly 1.972, so the free surface release features would occur at 1550 and 22 m/s. The actual free surface features occur at 1506 and 68 m/s, which differs from the elastic calculation, though much less so than in experiment SSD6. Slight decreases in the fringe amplitude during shock transit confirm that the material is deforming inelastically. Since the signs of inelastic behavior are subtle, it is quite likely that this experiment is slightly over the elastic limit.

3.3.4 Experiment SSD10

To study purely elastic compression states in diamond, a revised launch system was devised for the two-stage gun. The first stage was circumvented by a compressed gas bottle, which drove the second stage projectile directly. With this method, it was possible to obtain velocities below 1 km/s, although the actual velocity was quite variable from shot to shot. Two experiments not shown here (SS9 and SSD11) had extremely bizarre PDV data, with considerable motion just prior (< 1000 ns) to high frequency fringing; projectile failure,

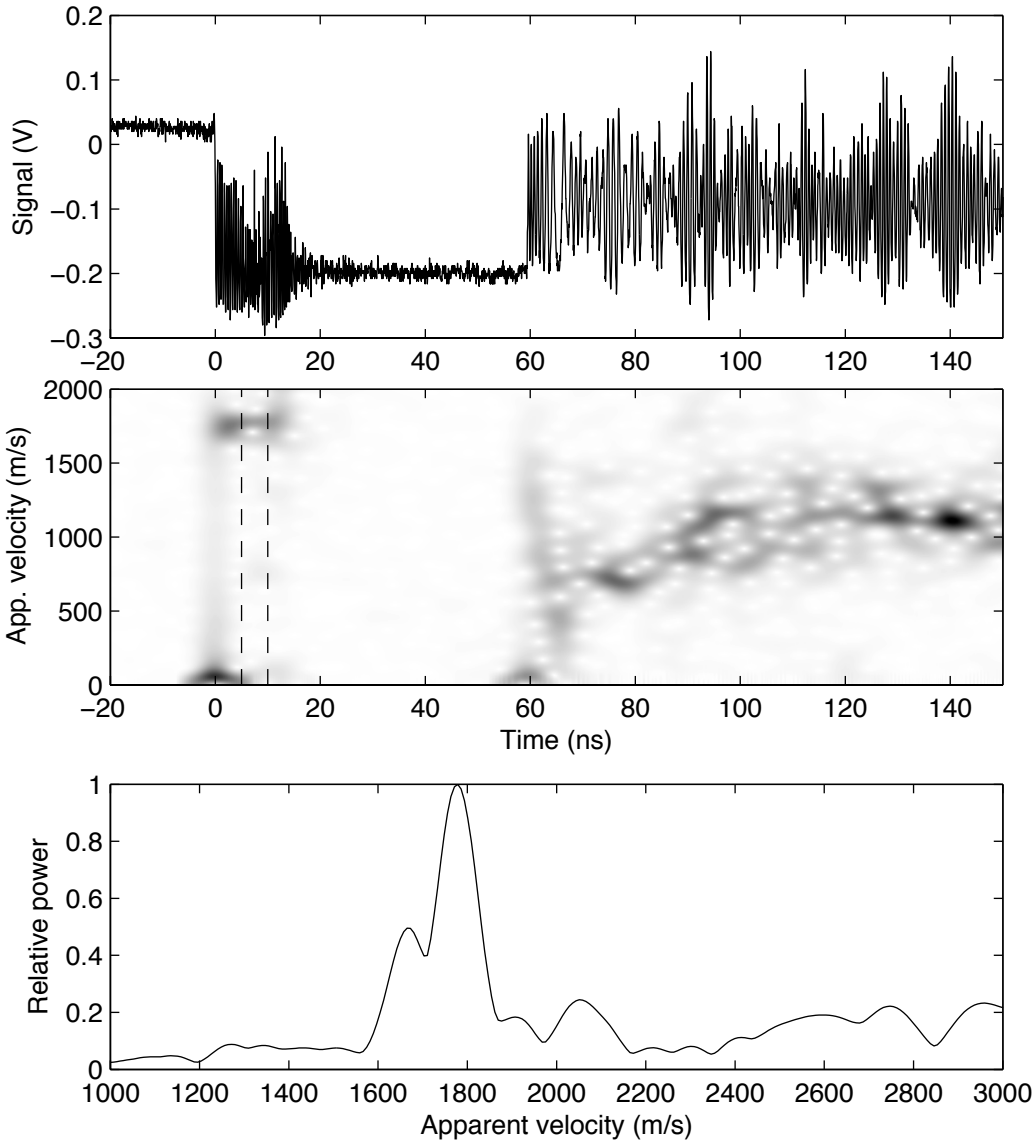

Figure 3.6. PDV results for experiment SSD7

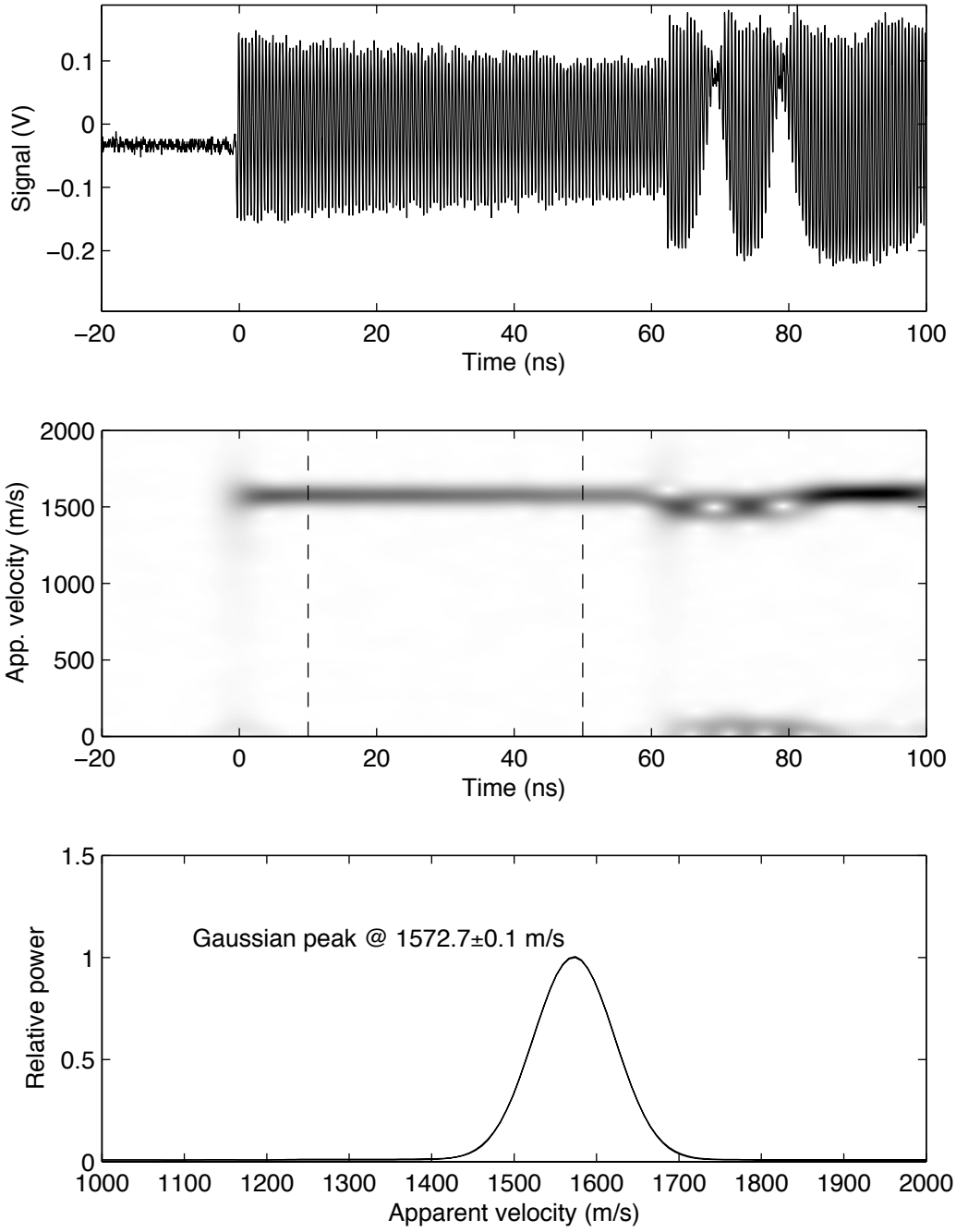

Figure 3.7. PDV results for experiment SSD8

with debris striking the target at multiple times, is a possible explanation. One experiment, SSD10, was successfully performed in this non-standard configuration. The measured impact velocity was 971 m/s.

Figure 3.8 shows the results for this experiment, analyzed in the same fashion as experiment SSD6. After impact, the PDV signal indicates a steady apparent velocity of 970.9 ± 0.8 m/s for a duration of 71.4 ± 0.1 ns ns, at which point free surface motion begins. Applying analysis described in experiment SSD6, the window correction is roughly 2.000, so the free surface release features would occur at 971 and 0 m/s. The actual free surface features occur at 939 and 45 m/s, which still differs from the elastic calculation. This difference is somewhat surprising because the PDV fringe amplitude does not vary substantially. Furthermore, the estimated stress (using Boteler's model) is 33 GPa, which is well within the region of reversible compression [9].

3.3.5 Summary of PDV measurements

Four symmetric impact experiment were successfully performed with PDV measurements. One experiment (SSD7) showed clear signs of inelastic deformation: the sample became opaque after shock compression. Two other experiments (SSD6 and SSD8) showed more subtle light light loss, and the predicted and measured velocity signatures after free surface release were not consistent. However, a similar inconsistency was also found at much lower pressures (SSD10, 33 GPa), where diamond is thought to be elastic.

3.4 Analysis and results

The shock compression behavior of synthetic diamond can be inferred from the VISAR and PDV measurements described above. For the purposes of this project, only the elastic range is of interest, since this is where synthetic diamond would be useful as a dynamic compression window. To do this, the distinction between experiments containing elastic and inelastic behavior is made. Next, the mechanical behavior in shocked diamond in the elastic range is analyzed. Finally, the window corrections for diamond in the elastic range are calculated.

Table 3.2 summarizes shock analysis of the successful symmetric impact experiments (SSD3 is omitted from this list due to the un-physically large shock speed). The particle velocity u_p is determined from the impact velocity and the experiment symmetry ($u_p = v/2$). The shock velocity U_s is calculated from the transit time, assuming a single shock wave in the sample. Conservation of momentum:

$$P = \rho_0 U_s u_p \tag{3.1}$$

is used to determine the shock stress P. The apparent velocity u_p^* is obtained from the VISAR/PDV measurement.

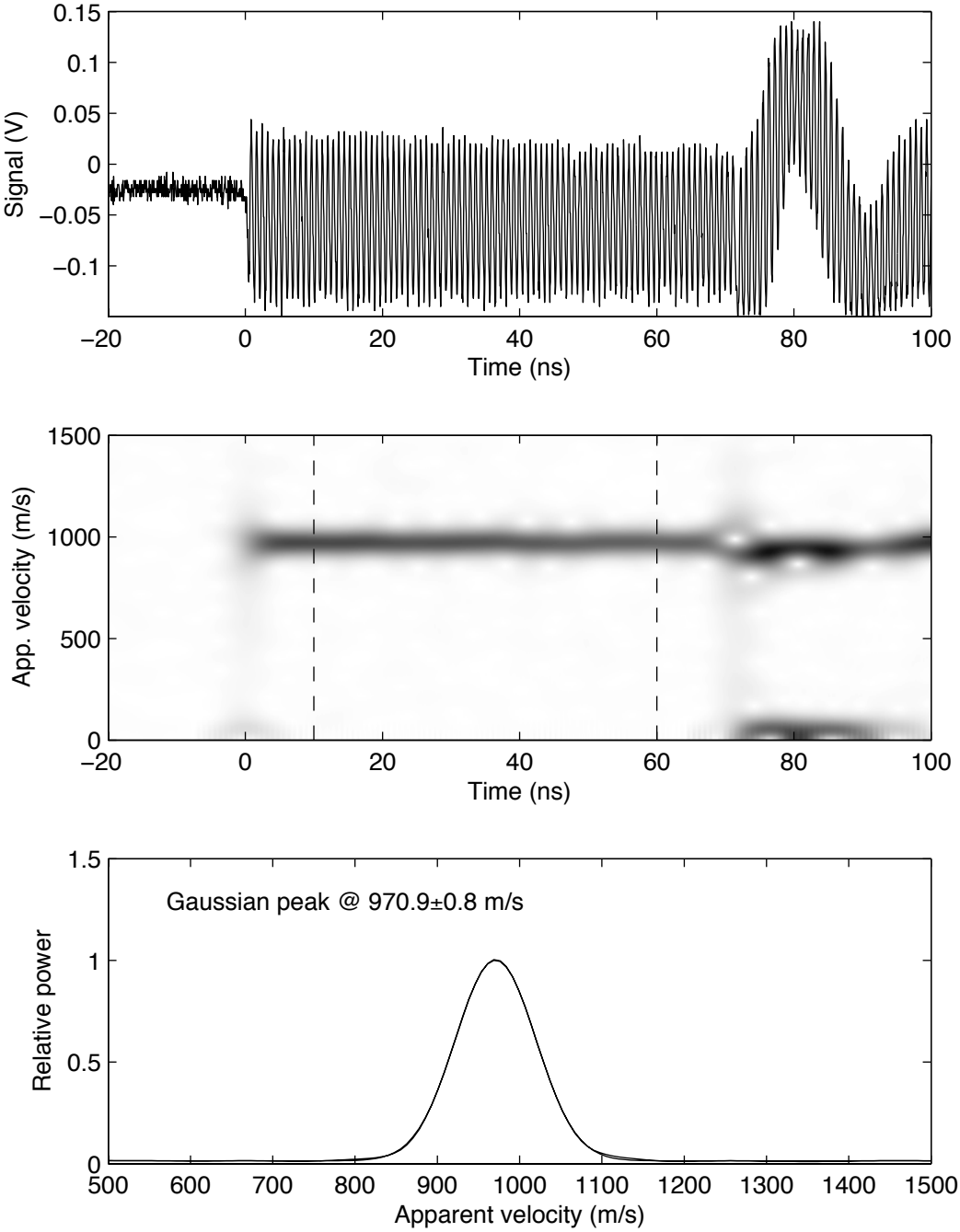

Figure 3.8. PDV results for experiment SSD10

Table 3.2. Shock analysis of symmetric impact experiments

Experiment	u_p (km/s)	U_s (km/s)	P (GPa)	u_p^* (m/s)
SSD1	0.800 ± 0.002	17.87 ± 0.10	50.4 ± 0.3	1.577 ± 0.011
SSD2	0.751 ± 0.002	18.39 ± 0.13	48.6 ± 0.3	1.474 ± 0.016
SSD6	0.846 ± 0.002	18.53 ± 0.10	55.2 ± 0.3	1.663 ± 0.002
SSD7	0.889 ± 0.002	18.32 ± 0.10	57.3 ± 0.3	1.779 ± 0.022
SSD8	0.797 ± 0.002	18.23 ± 0.08	51.2 ± 0.3	1.573 ± 0.000
SSD10	0.485 ± 0.001	19.13 ± 0.07	32.7 ± 0.1	0.971 ± 0.001

3.4.1 The elastic domain

A key trait of elastic compression—when the diamond window remains transparent during shock compression—is observed experiments SSD1, SSD2, and SSD10. SSD7 is a clear example of inelastic compression because of the onset of opacity; SSD6 and SSD8 are probably inelastic as well, though less obviously so.

Inelastic behavior might also be inferred by comparing apparent velocities after free surface release to estimates of an ideal, elastic material. For example, light reflected from the impact surface will have an apparent velocity of:

$$\begin{aligned} u^* &= au - (a-1)u_S \\ &\approx (2-a)u \qquad (u_S \approx 2u) \end{aligned} \tag{3.2}$$

after free surface release. This approximation is based on the idea that the free surface launches at twice the *in situ* particle velocity upon release. Deviations from this approximation are seen in every experiment described in the previous two sections. The discrepancy was pointed out directly in the PDV measurements, but can be seen directly in the VISAR record as well whenever $u^* < 0$. Negative apparent velocities can only occur when the window correction exceeds 2, but such values are not consistent with the apparent velocity before free surface release. The apparent contradiction may stem from inaccuracies in the free surface velocity assumption, something that deserves further study in the future.

3.4.2 Mechanical behavior of shocked diamond

Using the sample thicknesses, transit times, and impact velocities, it is possible to infer the Hugoniot state for each symmetric impact experiment. These values are displayed in Table 3.2 and plotted in Figure 3.9. Point obtained with VISAR measurements are shown with open circles, while points from PDV measurements are shown with open squares. For comparison, the Hugoniot created by Boteler [9] is shown as well (dashed line).

No obvious trend emerges in the calculated Hugoniot states. Experiments that should be completely elastic are far removed from Boteler's model, while clearly inelastic experiments

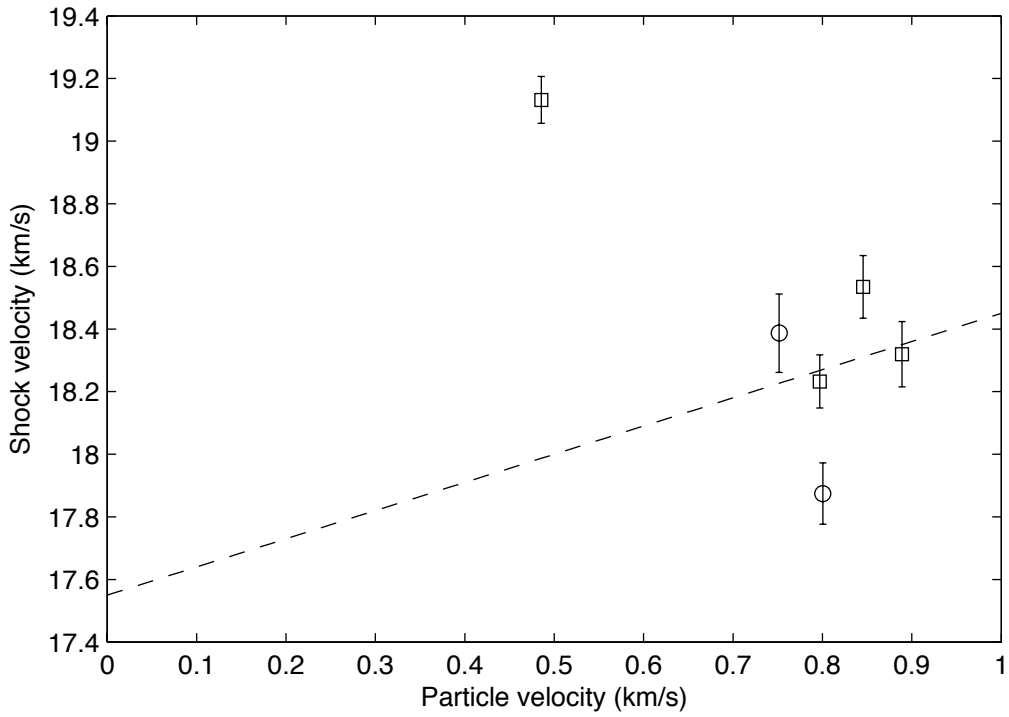

Figure 3.9. Calculated Hugoniot states for synthetic diamond

lie on the model Hugoniot. One interpretation is that all points to the right of 0.6 km/s are inelastic states, leaving only a single elastic point and an intermediate discontinuity; this interpretation requires a severe underestimate of the second order constants in Boteler's model.

Variation in the sample orientation is a possibility: perhaps the sample windows were insufficiently close to $\langle 100 \rangle$ to maintain consistent shock behavior? Sample purity is another variable to consider. Synthetic diamond typically retains 1–100 ppm of nitrogen, which is used to enhance the CVD growth rate. Lithium fluoride shows tremendous elastic sensitivity to impurities at the 100 ppm level [1], but the mechanical effects of residual nitrogen in synthetic diamond is not known. Further study is needed to understand the mechanical properties of synthetic diamond under shock compression.

3.4.3 Window correction

For a linear window material, the apparent velocity is proportional to the true velocity by a wavelength specific factor [24]. Essentially, the slope of u_p^* versus u (forced through the origin) defines the window correction in this situation. Figure 3.10 applies better this analysis to the four experiments thought to be elastic (SSD1, SSD2, SSD8, and SSD10). The estimated window correction for synthetic diamond is 1.966 (532 nm) and 1.981 (1550 nm). For comparison, the ambient refractive index of diamond [5] is 2.423 and 2.383 (respectively). This difference between window correction and refractive index is not unexpected [3], and results an increase of refractive index with density ($dn/d\rho > 0$).

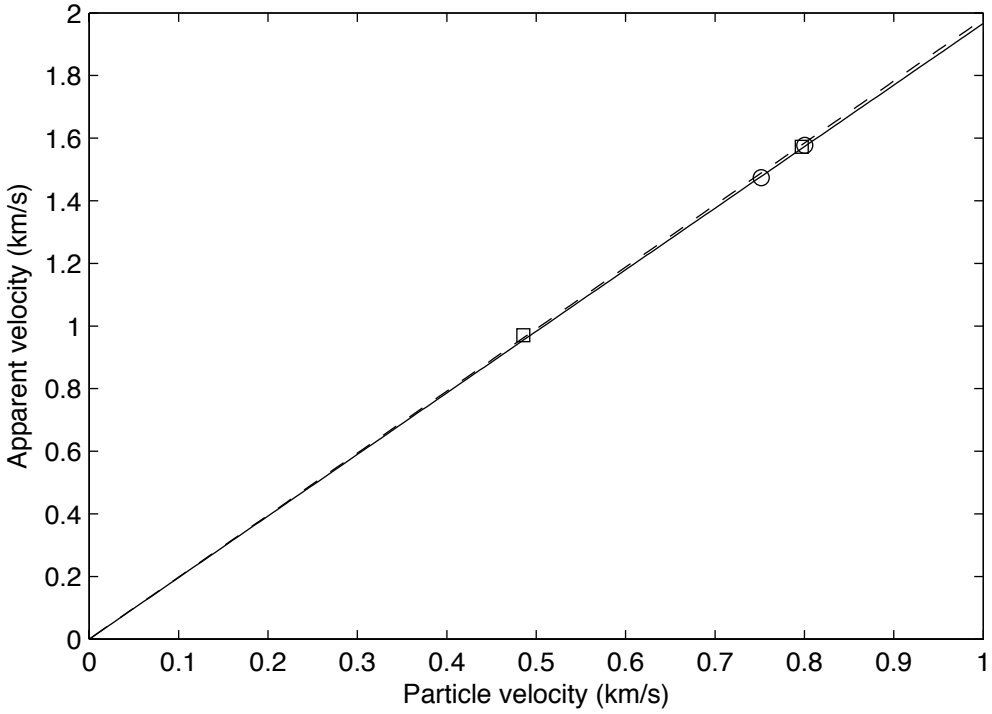

Figure 3.10. Apparent velocity corrections for synthetic diamond

CHAPTER 4
Ongoing research

Several areas of investigation launched during this project did not reach full completion. Two topics in particular—reverse impact experiments and three-phase PDV measurements—are described here in some detail. The reverse impact experiments revealed unexpected behavior in the two-stage gun. Three-phase PDV measurements were planned for the symmetric impact experiments, but due to schedule delays, were not available in time for the impact experiments. A new method for analyzing three-phase measurements was developed to for this project, and this method may find broader utility in other velocimetry measurements.

4.1 Alternate impact configurations

Several alternatives to symmetric impact were considered throughout this project. The motivation for these alternatives was to reduce the amount of diamond consumed in each shot, allowing more experiments to be performed (particularly near the elastic limit). Two concepts are presented here, one of which was attempted experimentally.

4.1.1 Concepts

By replacing the diamond impactor with a known material (*e.g.*, Al or Cu), one can infer the impact state through impedance matching [25]. Though not as precise as symmetric impact, impedance matching only requires a single diamond per experiment. Furthermore, the use of other materials relaxes the centering tolerances on the projectile because the impactor can be made much larger than the diamond sample.

The opposite of impedance matching, denoted here as reverse impact, was attempted in this project. A diamond impactor was launched onto a lithium fluoride window, with a VISAR diagnostic tracking the position of the impact surface. This configuration was selected because it eliminated the optical effects of diamond and because the projectile velocity could be increased to 2–3 km/s, where the two-stage gun is well behaved. A focusing VISAR probe was used to track the motion of a 1 mm diameter Al mirror on a 2 mm thick lithium fluoride window. No anti-reflective coating was needed in this measurement because the LiF window was thicker than the diamond target (both in real and virtual terms) and

had a much smaller free surface reflection.

4.1.2 Reverse impact trials

Several reverse impact attempts were made to study the shock behavior of synthetic diamond. Apart from the larger size of the lithium fluoride target, the reverse impact experiments were constructed in precisely the same fashion as the symmetric impact experiments described in the previous chapter. A fixed cavity VISAR, built by the Special Technologies Laboratory, was used in these experiments. Before each experiment, signal levels of 80–100 mV were obtained using un-amplified photodiodes. Due to the extremely high efficiency of the fixed cavity VISAR, a 2 W continuous laser provided sufficient light for the measurement.

Two diamond experiments, SSD12 and SSD13, were performed in the reverse impact configuration. In both cases, a dramatic loss of signal occurred at some point between the launch of the primary projectile and impact. This loss took place long before impact (at least 10 μs before), and is not related to reflectance changes that might occur during impact. A subsequent test was performed with a tantalum impactor launched onto a LiF-LiF stack, with the mirror confined between the windows. No dramatic intensity changes were detected in this experiment, suggested that bare Al coatings may become degraded prior to impact on the two-stage gun. The nature of this degradation is not understood, but might be a result of gas blow-by around the secondary projectile, which abrades the reflector off of the target. All symmetric impact experiments utilized a bare window, but severe signal degradation was only observed in the reverse impact experiments, so the effect may be tied to the lithium fluoride window. Apart from the target's composition, the only difference between the symmetric and reverse impact experiments is that the latter used a small diameter reflector (1 mm) while the former was fully coated on one side.

Additional reverse impact experiments were postponed pending a better understanding of how to avoid signal degradation. Protective buffers are an option, though not an ideal solution because of the need for an epoxy bond. This bond can cause noticeable ringing in the velocimetry measurement, and is to be avoided if at all possible. Another solution might be to add a protective overcoat (such as 100 nm of silica) on top of the aluminum reflector. Whether such an overcoat is sufficient to protect the mirror from degradation remains to be seen.

4.2 Three-phase PDV measurements

Three-phase PDV measurements are a variation on standard PDV approaches to obtain quadrature information. Although implemented entirely in optical fiber components, the method is conceptually similar to the push-pull VISAR [26]. A three-phase PDV system was constructed for this project, though was not ready for use in actual experiments due to equipment failure. A brief overview of three-phase measurements is presented here, followed by a new analysis method that is relevant to the study of synthetic diamond windows. Finally, a hypothetical diamond experiment using the three-phase PDV is proposed.

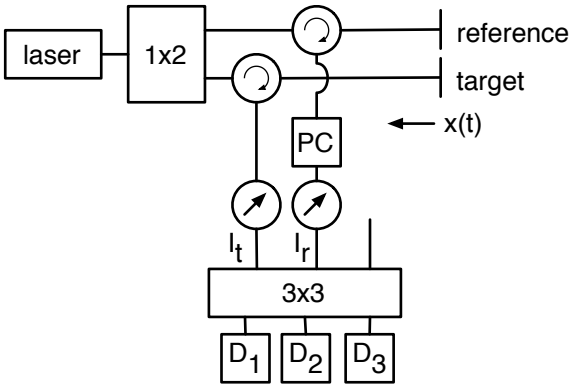

Figure 4.1. Conceptual layout for a three-phase PDV measurement

4.2.1 General principles

Figure 4.1 shows the conceptual layout of a three phase PDV measurement. The critical distinction between this layout and standard PDV is the use of a 3×3 coupler. The outputs of this component are phase-shifted by approximately 120°; the reason for this shift is described in Reference 27. The signals can be reduced to a quadrature pair, D_x and D_y, which define a set of perfect circles [28]. Much like VISAR measurements, the quadrature pair defines a phase shift that reveals the target velocity [29].

The weakness of three-phase PDV measurements in this project is that the method is optimally suited to single velocity measurements. Multiple velocities lead to a loss of contrast, much like in a VISAR, making it difficult or even impossible to extract a fringe shift. For the diamond measurements in this project, it is nearly impossible to avoid the presence of multiple apparent velocities. Diamond has a large refractive index, so there is a substantial free surface reflection (nearly 20%) for probes looking through this material. Since the windows are fairly thin ($\approx$ 1 mm),[1] it is difficult to separate the Al coated impact surface from the free surface. In fact, several round trips passages of light through the window can be be observed, similar to what has been reported in other window studies using PDV [21]. Since standard quadrature reduction cannot readily handle multiple input signals, along with cross-interference between these signals, a new reduction scheme is required.

4.2.2 Eliminating cross-interference

Consider a PDV measurement containing N optical signals, each with coherent intensity I_n, from the target under study. After mixed with the reference light, the total intensity

[1]The large refractive index of diamond makes the virtual thickness smaller, so the two surfaces appear closer together than they actually are.

measured by the detector is:

$$I = I_R + \sum_n I_n + I_E + 2\sum_{n=1}^{N} \sqrt{I_n I_R}\cos\Phi_{nR} + 2\sum_{n=1}^{N}\sum_{m=n+1}^{N} \sqrt{I_n I_m}\cos\Phi_{nm} \tag{4.1}$$

where I_R is the reference intensity, I_E is the total incoherent emission from the target, and Φ is the phase difference between two optical signals. The first sum is the interference of each target signal with the reference signal, while the second summation accounts for cross-interference between the different target signals. In general, it can be quite difficult to separate these two classes of interference in time-frequency analysis [21].

Three-phase measurements can be used to eliminate some of complexity from a multiple signal measurement. The phase shifts induced by the 3×3 coupler create phase shifts in the interference between the two input sources (target and reference), but not within a single source. As such, the signal measured by the k-th detector ($k = 1..3$) is:

$$\begin{aligned} D_k = a_k I_R + b_k \left(I_E + \sum_n I_n \right) \\ + 2\sqrt{a_k b_k}\sum_n \sqrt{I_R I_n}\cos(\Phi_{nR} - \beta_k) + 2\sqrt{a_k b_k}\sum_{n=1}^{N}\sum_{m=n+1}^{N} \sqrt{I_n I_m}\cos\Phi_{nm} \end{aligned} \tag{4.2}$$

where a_k is the coupling between the reference input and the detector, b_k is the coupling between the target input and the detector, and β_k is the phase shift from the 3×3 coupler. The signals can be normalized with respect to the static reference contribution; for AC coupled measurements, the subtraction of $a_k I_R$ is not necessary.

$$\begin{aligned} \hat{D}_k \equiv \frac{D_k - a_k I_R}{a_k I_R} \qquad \hat{b}_k \equiv \frac{b_k}{a_k} \qquad \hat{I} \equiv \frac{I}{I_R} \\ \hat{D}_k = \hat{b}_k \left(\hat{I}_E + \sum_n \hat{I}_n \right) \\ + 2\sqrt{\hat{b}_k}\sum_n \sqrt{\hat{I}_n}\cos(\Phi_{nR} - \beta_k) + 2\sqrt{\hat{b}_k}\sum_{n=1}^{N}\sum_{m=n+1}^{N} \sqrt{\hat{I}_n \hat{I}_m}\cos\Phi_{nm} \end{aligned} \tag{4.3}$$

For single velocity measurements, the three signals can be combined to eliminate the effects of time dependent target intensity [28]. An similar approach can be used to eliminate cross-interference.

To eliminate cross-interference, consider scaled differences between the normalized sig-

nals, using the convention that D_2 leads D_1 by β_+ and D_3 lags D_1 by β_-.

$$Q_2 \equiv \frac{\hat{D}_2}{\sqrt{\hat{b}_2}} - \frac{\hat{D}_1}{\sqrt{\hat{b}_1}} \tag{4.4}$$
$$= \left(\sqrt{\hat{b}_2} - \sqrt{\hat{b}_1}\right)\left(\hat{I}_E + \sum_n \hat{I}_n\right) + 2\sum_n \sqrt{\hat{I}_n}\left[(\cos\beta_+ - 1)\cos\Phi_{nR} - \sin\beta_+ \sin\Phi_{nR}\right]$$
$$Q_3 \equiv \frac{\hat{D}_3}{\sqrt{\hat{b}_3}} - \frac{\hat{D}_1}{\sqrt{\hat{b}_1}} \tag{4.5}$$
$$= \left(\sqrt{\hat{b}_3} - \sqrt{\hat{b}_1}\right)\left(\hat{I}_E + \sum_n \hat{I}_n\right) + 2\sum_n \sqrt{\hat{I}_n}\left[(\cos\beta_- - 1)\cos\Phi_{nR} + \sin\beta_- \sin\Phi_{nR}\right]$$

The parameters needed for these constructions may be obtained from beam-block measurements, and depend entirely on the operation of the 3×3 coupler. Quadrature signals can be obtained from combinations of Q_2 and Q_3.

$$D_x \equiv \sin\beta_-\ Q_2 + \sin\beta_+\ Q_3 = \sum_k g_k \hat{D}_k$$
$$= A\left(\hat{I}_E + \sum_n \hat{I}_n\right) + C\sum_n \sqrt{\hat{I}_n}\cos\Phi_{nR} \tag{4.6}$$
$$D_y \equiv -(\cos\beta_- - 1)Q_2 + (\cos\beta_+ - 1)Q_3 = \sum_k h_k \hat{D}_k$$
$$= B\left(\hat{I}_E + \sum_n \hat{I}_n\right) + C\sum_n \sqrt{\hat{I}_n}\sin\Phi_{nR} \tag{4.7}$$
$$A = \sin\beta_-\left(\sqrt{\hat{b}_2} - \sqrt{\hat{b}_1}\right) + \sin\beta_+\left(\sqrt{\hat{b}_3} - \sqrt{\hat{b}_1}\right)$$
$$B = (1 - \cos\beta_-)\left(\sqrt{\hat{b}_2} - \sqrt{\hat{b}_1}\right) + (\cos\beta_+ - 1)\left(\sqrt{\hat{b}_3} - \sqrt{\hat{b}_1}\right)$$
$$C = 2\left[\sin\beta_-(\cos\beta_+ - 1) + \sin\beta_+(\cos\beta_- - 1)\right]$$

The summation weights for the quadrature function are as follows.

$$g_1 = -\frac{\sin\beta_- + \sin\beta_+}{\sqrt{\hat{b}_1}} \qquad g_2 = \frac{\sin\beta_-}{\sqrt{\hat{b}_2}} \qquad g_3 = \frac{\sin\beta_+}{\sqrt{\hat{b}_3}}$$
$$h_1 = \frac{(\cos\beta_- - 1) - (\cos\beta_+ - 1)}{\sqrt{\hat{b}_1}} \qquad h_2 = \frac{-(\cos\beta_- - 1)}{\sqrt{\hat{b}_2}} \qquad h_3 = \frac{(\cos\beta_+ - 1)}{\sqrt{\hat{b}_3}}$$

For an ideal 3×3 coupler, both phase shifts are precisely $120°$ and $\hat{b}_k = 1$, which leads to a simple quadrature reduction.

$$D_x = 2\hat{D}_1 + \hat{D}_2 + \hat{D}_3$$
$$D_y = \sqrt{3}\left(\hat{D}_2 - \hat{D}_3\right) \qquad \text{(ideal)}$$

This form of quadrature reduction is equivalent to single velocity reduction in the ideal case [28] after sign inversion of signals D_2 and D_3. In general, the actual values of g_k and h_k might be needed to properly balance the quadrature signals, but the ideal form might be suitable in many cases since arctangent inversion is not used.

To understand the utility of quadrature reduction in this setting, note that the constants A and B are much smaller than C; for ideal coupler, A and B are both zero while $C = 3\sqrt{3}$. As a result, the non-interfering portions of Equations 4.6 and 4.7 drop out.

$$D_x = C \sum_n \sqrt{\hat{I}_n} \cos \Phi_{nR} \tag{4.8}$$

$$D_y = C \sum_n \sqrt{\hat{I}_n} \sin \Phi_{nR} \tag{4.9}$$

The above statements are approximately true for a non-ideal coupler if the reference intensity is larger than the total light received from the target (coherent and incoherent). Therefore, this form of quadrature reduction separates target-reference interference from cross-interference and removes baseline variations. The two signals can be further combined into an imaginary signal:

$$\tilde{D} \equiv -iD_x + D_y = -iC \sum_n \sqrt{\hat{I}_n} e^{-i\Phi_{nR}}, \tag{4.10}$$

which as a real Fourier transform. At the very least, this process reduces the number of Fourier transforms needed in time-frequency analysis, and could improve the signal-noise ratio somewhat (as compared to single channel analysis). Whether a particular form of time-frequency analysis could capitalize on the transform properties of $\tilde{D}$ remains to be seen.

An important consideration in quadrature reduction is the possible amplification of signal noise. If the normalized signal error is $\delta\hat{D}$, then signal-noise ratio on one signal is:

$$\rho_1 = \frac{\Delta\hat{D}_1}{\delta\hat{D}} = \frac{4\sqrt{\hat{I}_n}}{\delta\hat{D}} \tag{4.11}$$

where $\sqrt{\hat{I}_n}$ is the weight of single coherent term. Applying similar analysis to quadrature signals, assuming a perfect 3×3 coupler, yields a similar result.

$$\rho_x = \frac{\Delta\hat{D}_x}{\delta D_x} = \frac{2 \cdot 2\sqrt{3}\sqrt{\hat{I}_n}}{\sqrt{6}\ \delta\hat{D}} = \frac{3\sqrt{2}}{4}\rho_1 \tag{4.12}$$

Quadrature reduction therefore has slightly better (about 6%) signal-noise than the original data signals. Combining the two quadrature signals into a complex-valued signal might further reduce noise effects, the precise effect is not obvious. At the very least, separate time-frequency analysis of the quadrature signals could be averaged to improve noise performance.

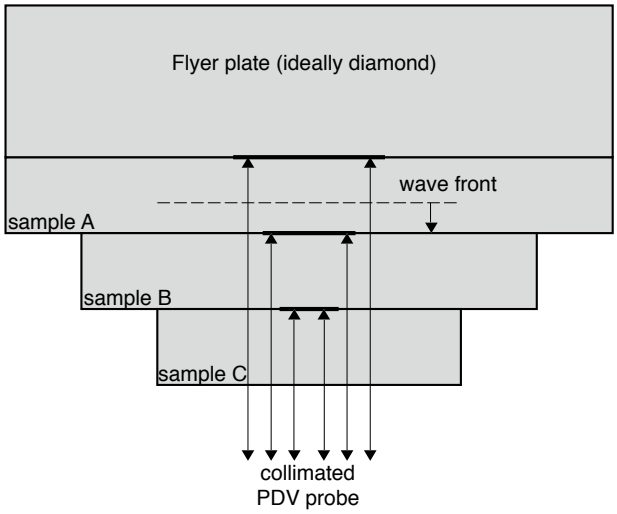

Figure 4.2. Multi-layer PDV measurement concept

4.2.3 Multi-layer PDV measurements in diamond

A potential application of revised quadrature analysis is illustrated in Figure 4.2. In this experiment, multiple material layers (A, B, and C) are bonded together. An impact plate (ideally diamond itself) is launched onto the first sample, generating a shock wave. As the wave propagates through the sample, reflectors deposited at each material interface begin are accelerated. By varying the reflector diameter between layers (or using offset mirror sections), it is possible to track the motion of each interface with a single PDV probe.

Analysis of a conventional PDV measurement would be extremely complicated due to the cross-interference between different material layers. Revised quadrature reduction, however, would simplify this process tremendously.

CHAPTER 5

Summary

The overall goal of this project was to determine whether synthetic diamond could be used as a dynamic compression window. Based on the results thus far, diamond might be useful in many circumstances, but several important questions remains unanswered. The following sections summarize the project results, describe some of the ongoing efforts related to this project, and provide recommendations for future work in this area.

5.1 Project summary

Symmetric impact experiments were used to characterize the shock response of synthetic diamond. Velocimetry (VISAR and PDV) measurement probed the wave transit in diamond during the experiments, and provided information about the material's optical properties. A range of impact velocities were obtained with standard and non-standard configurations of the STAR two-stage gun.

A few impact experiments show clear signs of inelastic behavior, indicating areas where diamond would not be a useful window material. For the $\langle 100 \rangle$ orientation, the upper useful limit is below 57 GPa, possibly as low as 51 GPa. Qualitative elastic behavior is observed in several VISAR and PDV measurements at lower stresses, but no consistent Hugoniot emerges from this data. Furthermore, subtle details of the free surface release suggest non-elastic behavior in the seemingly elastic experiments. Release state inconsistencies may stem from an inappropriate approximation in the calculated apparent velocity.

The window correction for synthetic diamond is just under 2 (1.966 at 532 nm, 1.981 at 1550 nm). These values are larger than the corrections for any other dynamic window material.

5.2 Ongoing work

Reverse impact experiments, where diamond is launched into a lithium fluoride window, were tried to reduce the amount of diamond consumed in each shot. Catastrophic light loss during projectile launch was observed in each reverse impact attempt. It was determined

that this loss comes long before impact, and is tied to the use of an exposed target mirror; when this mirror was covered with a buffer, the effect disappeared. Neither the mechanism nor a universal solution to this problem has been identified.

A three-phase PDV system was constructed for use in this project, but due to equipment failures was not used in the experiments. However, a new quadrature reduction scheme was developed to optimally use three-phase PDV in multiple velocity measurements.

5.3 Recommendations for future work

Since synthetic diamond has a tremendous potential as a window for shock and ramp wave compression experiments, further study of this material is clearly warranted. Based on the results of this work, future studies should consider the following issues.

- Sample dimensions
  A significant problem in this project was the limited size, parallelism, and shape of the diamond samples. Over time, the situation has improved, though larger samples (6–12 mm diameter) would to reduce impact centering requirements.

- Sample purity, treatment, and characterization
  As synthetic diamond becomes more common, standard purity and quality tolerances should be established for dynamic compression windows. Guidelines for the use of high pressure, high temperature annealing treatments (if any) should also be defined.

- Probe design and alignment
  In at least one experiment of this project, the velocimetry probe pointed far from the sample center. A robust probe design is needed to ensure the proper probe centering. Tilt compensation might also be needed for PDV probes, where the fiber is angle polished.

- Controlled impactor launch below 1.5 km/s
  Modest velocities (0.50–1.00 km/s) are needed to study the elastic behavior of diamond using symmetric impact. However, it is crucial that the projectile remain precisely centered (< 0.100 mm) during the experiment. At the same time, the launcher must not degrade exposed mirrors on the target's impact surface. No existing launcher at Sandia routinely achieve all of these conditions.

The issue of sample size may be the most important of these recommendations because it affects most of the other issues. With larger diamond samples, the experiment and diagnostic design tolerances could be relaxed.

In the near term, significant progress could be made by focusing experiments in below 40 GPa, where $\langle 100 \rangle$ diamond is thought to be elastic. Impedance matching experiments, using large aluminum, copper, or even sapphire impactors, might be the best approach for pinning down the elastic properties of synthetic diamond.

References

[1] J. Asay, G. Fowles, G. Duvall, M. Miles, and R. Tinder, "Effects of point defeces on elastic precursor decay in LiF," *Journal of Applied Physics* **43**, 2132 (1972).

[2] Y. Gupta, "Effect of crystal orientation on dynamic strength of LiF," *Journal of Applied Physics* **48**, 5067 (1977).

[3] D. Dolan and T. Ao, "Cubic zirconia as a dynamic compression window," *Applied Physics Letters* **93**, 21908 (2008).

[4] M. Knudson, J. Asay, S. Jones, and Y. Gupta, "Shock response of diamond crystals," Tech. Rep. SAND2001-3838, Sandia National Laboratories (2001).

[5] E. Palik (editor), *Handbook of Optical Constants of Solids* (Academic Press) (1985).

[6] A. Jayaraman, "Diamond anvil cell and high-pressure physical investigations," *Reviews of Modern Physics* **55**, 65 (1983).

[7] A. Jayaraman, "Ultrahigh pressures," *Review of Scientific Instruments* **57**, 1013 (1986).

[8] J. Boteler and Y. Gupta, "Shock induced splitting of the triply degenerate Raman line in diamond," *Physical Review Letters* **71**, 3497 (1993).

[9] J. Boteler and Y. Gupta, "Raman spectra of shocked diamond single crystals," *Physical Review B* **66**, 14107 (2002).

[10] S. Zybin, M. Elert, and C. White, "Nanoscale view of shock-wave splitting in diamond," *Metallurgical and Materials Transactions A* **35A** (2004).

[11] L. Barker and R. Hollenbach, "Laser interferometer for measuring high velocities of any reflecting surface," *Journal of Applied Physics* **43**, 4669 (1972).

[12] R. Hazen, *The diamond makers* (Cambridge University Press) (1999).

[13] A. Collins, *The nature of diamonds*, chap. Diamonds in modern technology: synthesis and applications (Cambridge University Press) (1998).

[14] J. Daivs, "The new diamond age," *Wired* (2003).

[15] C. Yan, Y. Vohra, H. Mao, and R. Hemley, "Very high growth rate chemical vapor deposition of single-crystal diamond," *Proceedings of the National Academy of Sciences* **99**, 12523 (2002).

[16] `http://www.carnegieinstitution.org/diamond-13may2005/`.

[17] J. Boteler, *Time resolved Raman spectroscopy in diamonds shock compressed along [110] and [100] orientations*, Ph.D. thesis, Washington State University (1993).

[18] S. Jones and Y. Gupta, "Refractive index and elastic properties of z-cut quartz shocked to 60 kbar," *Journal of Applied Physics* **88**, 5671 (2000).

[19] S. Jones, M. Robinson, and Y. Gupta, "Ordinary refractive index of sapphire in uniaxial tension and compression along the c axis," *Journal of Applied Physics* **93**, 1023 (2003).

[20] B. Lalone, O. Fat'yanov, J. Asay, and Y. Gupta, "Velocity correction and refractive index changes for [100] lithium fluoride optical windows under shock compression, recompression, and unloading," *Journal of Applied Physics* **103**, 93505 (2008).

[21] B. Jensen, D. Holtkamp, P. Rigg, and D. Dolan, "Accuracy limits and window corrections for photon Doppler velocimetry," *Journal of Applied Physics* **101**, 13523 (2007).

[22] T. Thornhill, W. Reinhart, C. Konrad, and L. Chhabildas, "Accurate velocity measurments of the two-stage light-gas gun projectile," Tech. Rep. SAND2000-2268C, Sandia National Laboratories (2000).

[23] O. Fat'yanov, R. Webb, and Y. Gupta, "Optical transmission through inelastic deformed shocked sapphire: stress and crystal orientation effects," *Journal of Applied Physics* **97**, 123529 (2005).

[24] D. Dolan, "Foundations of VISAR analysis," Tech. Rep. SAND2006-1950, Sandia National Laboratories (2006).

[25] A. Mitchell and W. Nellis, "Shock compression of aluminum, copper, and tantalum," *Journal of Applied Physics* **52**, 3363 (1981).

[26] W. Hemsing, "Velocity sensing interferometer (VISAR) modification," *Review of Scientific Instruments* **50**, 73 (1979).

[27] R. Priest, "Analysis of fiber interferometer utilizing 3x3 fiber coupler," *IEEE Transactions on Microwave Theory and Techniques* **MTT-30**, 1589 (1982).

[28] D. Dolan and S. Jones, "Push-pull analysis of photonic Doppler velocimetry measurements," *Review of Scientific Instruments* **78**, 076102 (2007).

[29] D. Dolan and S. Jones, "THRIVE: a data reduction program for three-phase PDV/PDI and VISAR measurements," Tech. Rep. SAND2008-3871, Sandia National Laboratories (2008).

DISTRIBUTION:

1	MS 1195	S.C. Alexander, 1647
1	MS 1195	T. Ao, 1646
1	MS 1195	J.R. Asay, 1646
1	MS 1195	J.-P. Davis, 1646
5	MS 1195	D.H. Dolan, 1646
1	MS 1195	M.D. Furnish, 1647
2	MS 1195	C.A. Hall, 1646
1	MS 1159	S.C. Jones, 1344
1	MS 1195	M.D. Knudson, 1646
2	MS 1195	T. Mehlhorn, 1640
1	MS 1195	W.D. Reinhart, 1647
1	MS 1195	S. Root, 1646
1	MS 9042	T.J. Vogler, 8776
1	MS 1195	J. Wise, 1646
1	MS 0899	Technical Library, 9536 (electronic)
1	MS 0123	D. Chavez, LDRD Office, 1011

Sandia National Laboratories